ORIGINAL PAPER

Sudden wave flooding on steep rock shores: a clear but hidden danger

Henrik Kalisch[1] · Francesco Lagona[2] · Volker Roeber[3,4]

Abstract

It is shown that very steep coastal profiles can give rise to unexpectedly large wave events at the coast. We conduct a statistical analysis of runs from a nearshore Boussinesq-type model to demonstrate that under certain wave conditions, which a casual observer would perceive as calm, the likelihood of large run-up events is uncharacteristically high. The data computed by the Boussinesq-type model show that sea states with lower overall wave steepness favor higher run-up. Under these wave conditions, more of the available wave energy reaches the shore, since less wave breaking occurs, which can create a false sense of security for beach-goers.

Keywords Rock coast · Steep bathymetry · Wave run-up · Rayleigh distribution

1 Introduction

In the present work, we are interested in the interaction of ocean waves with steep coastal topography such as encountered in some rock coasts in the USA (Alaska and Maine), in Norway and in New Zealand. While steep rock coasts have been traditionally less studied due to the inherent challenges, they have recently moved into focus due to improved surveying technology and increasing pressure for commercial development (Kennedy et al.

Francesco Lagona and Volker Roeber have contributed equally to this work.

✉ Henrik Kalisch
  henrik.kalisch@uib.no

  Francesco Lagona
  francesco.lagona@uniroma3.it

  Volker Roeber
  volker.roeber@univ-pau.fr

[1] Department of Mathematics, University of Bergen, PO Box 7800, 5020 Bergen, Norway

[2] Department of Political Sciences, University Roma Tre, 00145 Rome, Italy

[3] E2S-UPPA, Chair HPC-Waves, SIAME, Université de Pau et des Pays de l'Adour, 64600 Anglet, France

[4] Department of Oceanography, University of Hawaii at Manoa, Honolulu 96822, USA

2014). Since many of these coasts were formed be retreating glaciers during the close of the last ice age, they are generally located far in the north or south. If global warming is to continue, then many more of such steep rock coasts will be exposed and more accessible in the future.

Rock coasts generally pose a greater risk to humans than sand or pebble beaches due to slippery conditions and the danger of being smashed onto hard rock by the waves and currents or due to a fall. If in addition, the sea floor slopes steeply up towards the shore, this risk is compounded by the sudden and unexpected appearance of large waves which seem completely out of proportion when compared to sea conditions visible to an observer. Such waves may suddenly flood a good portion of the rocks, potentially knocking by-standers off their feet and washing them into the sea in the back rush.

It is well established in the local lore on the Norwegian west coast that sudden large run-up may occur, though the conditions are often mischaracterized as stormy or soon after a storm. While stormy conditions are always dangerous, outlier events may happen under any conditions, and some reports indicate sever weather conditions. The most dangerous waves are swell waves from distant storms which may occur when local weather conditions are benign. In particular, long waves of small steepness are able to penetrate the many shoals off the coast without significant energy loss through wave breaking. When these long swells hit the steeply sloping coastal bathymetry, very large run-up may occur without any warning (Bjørnestad and Kalisch 2020).

Indeed, periodically news stories appear about people being washed into the sea by large and unexpected waves. One case which made international headlines, was the perishing of two members of a film crew (Roxborough 2011) in Egersund, Norway, after being washed into the sea by a large wave. Investigating the bathymetry near the film set shows a steep 1.5 : 1 slope that is actually steepening towards the shore. An in-depth look at the bathymetry along the Norwegian coast reveals that similar geometries occur in many places.

Many reported occurrences of freak waves and in particular extreme run-up events similar to what happened in Egersund have been compiled in a recent work (Didenkulova 2020). In a more recent work (Didenkulova et al. 2023), the authors have matched some of these events with meteorological background conditions.

Fig. 1 Photographs of wave conditions at the Norwegian coast near Haugesund at 59.48° N, 5.23° E on Jan. 29th, 2020 around 12:00 pm CET. Significant waveheight was estimated at 1 m. As seen in the left panel, conditions were rather calm. However, 20 seconds later significant run-up with nearly complete flooding of the top of the rock occurred (Bjørnestad and Kalisch 2020)

In the recent study (Bjørnestad and Kalisch 2020) focusing on the Norwegian coast near Haugesund, it was shown that uncharacteristically large run-up may occur in relatively calm conditions (see Fig. 1). This study was based on observations and a mathematical formulation of an exact solution of the shallow-water equations near the shore. The physical mechanism behind these large run-up events is the extreme amplification of the waves on the steep bathymetry. The amplification is so swift that the wave does not break before the wavecrest reaches the shoreline, resulting in a large run-up event. While the shallow-water model is able to capture the basic mechanism, in the present work, we use a more versatile model, the Boussinesq Ocean & Surf Zone model, *BOSZ* (Roeber and Cheung 2012) which incorporates both a shallow-water model as well as a dispersive Boussinesq model, and is able to give more detailed information. Using a large number of numerical runs with the *BOSZ* model, we then analyze the data, and show that indeed the distribution of run-up heights has very heavy tails, indicating that outlying events are more likely to happen than in a traditional probability distribution.

There are many empirical run-up formulas for beaches and coastal structures. Many of the early attempts to devise run-up relations used the Iribarren number (also called surf-similarity parameter)

$$\xi_f = \frac{\tan(\beta)}{\sqrt{H/L}}, \tag{1}$$

where β is the beach slope, H is a characteristic offshore waveheight and L is a characteristic wavelength. For example, (Holman 1986) defined a run-up model using the quantity $R_{2\%}$ which is the run-up height exceeded by 2% of the waves arriving at the beach. The most popular measure used on gentle beaches today is probably the Stockdon number (Stockdon et al. 2006) which is a variation on the relation found in Holman (1986).

These definitions are all based on the assumption that the beach is gently sloping. Some work has been done for steep beaches. In particular, (Ahrens 1981) did experiments with several steep slopes, and found the formula

$$\frac{R_{2\%}}{H_s} = C_1 + C_2\xi + C_3\xi^2, \tag{2}$$

where the constants C_1, C_2 and C_3 need to be determined on a case-by-case basis. In several cases, the constant C_3 is zero, and the run-up height increases linearly with significant waveheight.

In the present contribution, we use the Boussinesq Ocean and Surf Zone (*BOSZ*) model, a phase-resolving nearshore wave model based on the Nwogu (1993) equations to create a dataset of waves running up on a steel model slope. We use statistical analysis to identify the resulting distribution of wave-by-wave run-up height. We compare with both offshore distribution of waveheight and between steep and gently sloping shores. In order to deal with the steep bathymetry, we introduce some modifications regarding the treatment of breaking waves in the *BOSZ* model. The plan of the paper is as follows: In Sect. 2, we outline the numerical method to be used for the shoaling and run-up computations. In Sect. 3, the numerical experiments are described and the statistical analysis is detailed. Finally, Sect. 4 contains an in-depth discussion of the results.

2 Numerical methods

2.1 Overview

The *BOSZ* model was introduced in Roeber et al. (2010) and Roeber and Cheung (2012) and has been under continuous development for the last ten years. Numerous modules with various boundary conditions, wave generation tools and alternative numerical methods have been added on. The BOSZ model has been shown to yield accurate results in various situations. In particular, the model has been validated with laboratory data in Roeber and Cheung (2012a) and Wong et al. (2019). The model has also been validated with data from field campaigns (Li et al. 2014), as well as very recent campaigns in Varing et al. (2020) and Pinault et al. (2022). Moreover, the model output has been compared with other popular Boussinesq models in Roeber and Bricker (2015) and in Lynett et al. (2017), and even for ship waves (David et al. 2017). The basic idea behind the *BOSZ* model is the combination of the shock-capturing capabilities of the conserved nonlinear shallow-water equations with the qualities of Boussinesq-type equations to provide an accurate and stable solution of wave-by-wave propagation, transformation, breaking and run-up. The *BOSZ* model is based on a set of Boussinesq-type equations, of which the classical shallow-water equations are a subset, with additional terms accounting for pressure correction due to frequency dispersion. This enables the model to handle short (dispersive) waves and transitions between sub- and supercritical flow (wave breaking).

The governing equations of the model are intentionally kept as simple as possible with focus on the terms which govern the dominant processes of nearshore waves.

2.2 Wave breaking

Wave breaking in Boussinesq-type models has been an open debate for many years. As most governing equations are not catering to flow discontinuities due to their parabolic structure, the correctly converged solution over a refined grid would be a singularity (blowup). Obviously, the mathematically correct solution is not the desired solution from the user perspective—especially, since Boussinesq-type equations can provide reasonable answers across the entire surf zone and even for wave run-up (Pinault et al. 2020). Multiple methods have been proposed to handle this problem. In general, they utilize two opposing strategies: (a) Addressing the potentially arising singularity through a diffusive term based on the eddy viscosity concept; (b) Eliminating the singularity by locally recovering a hyperbolic solution through deactivation of the dispersion terms in the governing equations. Both approaches alter the governing equations temporarily and locally, with the former method adding terms and the latter one removing terms.

Option (b) has become a standard procedure in several operational models such as detailed in Shi et al. (2012) and in Roeber and Cheung (2012). However, the locally sudden change between dispersive and non-dispersive solutions can pose problems and instabilities when the grid size is small and a breaking wave is described over multiple grid cells (Kazolea and Ricchiuto 2018). Stable solutions therefore often rely on some degree of grid diffusion; hence, it is difficult to obtain converging results with a refined mesh.

The eddy viscosity concept (a), on the other hand, is based on applying an additional diffusion term to the cells across the wave breaking zone. This procedure is attractive, since the governing equations remain intact and no incompatibility arises from local deactivation of

dispersion terms. The eddy viscosity term counter balances the potentially arising instability along the wave front. It can be seen as a way to overcome the problem of the lack of 3D turbulence effects in the depth-integrated governing equation which naturally only allow for discontinuities and not for overturning of the free surface. While the diffusion terms are relatively straightforward to understand, the assessment of the magnitude of dissipation remains a challenge.

It is important to notice that without any interference the solution of the Boussinesq-type equations approach a singularity at a discontinuity if the numerical solution does not clip or diffuse the local values. Obviously, in this case, the mathematically correct solution is neither realistic nor it is the desired solution from the user perspective, especially since Boussinesq-type equations normally provide reasonable answers across the entire surf zone.

Here, we present one possible solution for closure of the eddy viscosity term through the calculation of an additional governing equation for turbulent kinetic energy. The temporal adjustment of the diffusion terms over the entire surf zone leads to converging results even with fine grids and enables the use of small grid sizes for accurate tracking of wave run-up over wet/dry slopes.

2.3 Identification of wave breaking onset

It is notoriously difficult to identify the onset of wave breaking in depth-integrated models since the free surface cannot overturn. Due to the constant balance of nonlinearity and dispersion, the numerical solution does not accurately describe the free surface near the wave breaking front. Recent advances based on potential flow models have shown that kinematic and dynamic criteria work more reliably to identify the breaking onset than formerly used geometric criteria (Barthelemy et al. 2018) which mostly use the free surface slope as indicator for wave breaking (Varing et al. 2021).

It should also be noted that stability along the breaking front is of priority in depth-integrated models, where wave breaking always remains an approximation. Here, we introduce an approach of how to address the potentially arising instabilities along the wave front inspired by the preliminary work (Nwogu 1996). The strategy is based on the *free surface Froude-Number*, which can be determined from the flow velocities in the equation found in Nwogu (1993). The quadratic assumption of the velocity profile is inherent to the governing equations and allows for calculation of the flow velocity at any position in the water column as

$$
\begin{aligned}
u|_\eta = u_{z_\alpha} &+ \frac{1}{2}\left(z_\alpha^2 - z^2\right)\left[\left(u_{z_\alpha}\right)_{xx} + \left(v_{z_\alpha}\right)_{xy}\right] \\
&+ \left(z_\alpha - z\right)\left[\left(hu_{z_\alpha}\right)_{xx} + \left(hv_{z_\alpha}\right)_{xy}\right], \\
v|_\eta = v_{z_\alpha} &+ \frac{1}{2}\left(z_\alpha^2 - z^2\right)\left[\left(u_{z_\alpha}\right)_{xy} + \left(v_{z_\alpha}\right)_{yy}\right] \\
&+ \left(z_\alpha - z\right)\left[\left(hu_{z_\alpha}\right)_{xy} + \left(hv_{z_\alpha}\right)_{yy}\right].
\end{aligned}
\tag{3}
$$

In one spatial dimension, the equation obviously reduces to

$$
u|_\eta = u_{z_\alpha} + \frac{1}{2}\left(z_\alpha^2 - z^2\right)\left(u_{z_\alpha}\right)_{xx} + \left(z_\alpha - z\right)\left(hu_{z_\alpha}\right)_{xx}.
\tag{4}
$$

Here, u_{z_α} is the horizontal flow speed at the reference depth z_α (around mid-depth), and h is the local water depth. With $z = \eta$, we obtain the horizontal flow velocity at the free surface

based on the approximations in Nwogu's equation. This approximation is reasonably valid as long as the waves are not strongly nonlinear and dispersive.

In general, the more dispersive the problem, the more the terms with second-order derivatives differ from zero. In contrast, for long-wave problems and near-hydrostatic solutions, the additional correction terms are not very significant and the velocity values at z_α are representative throughout the entire water column. It should also be noted that (3) and (4) involve second-order derivatives, which can potentially lead to numerically noisy solutions over variable terrain and for irregular wave fields.

The free surface Froude number can then easily determined from

$$Fr|_\eta = \frac{u|_\eta}{\sqrt{gh}}. \tag{5}$$

We know that for $Fr|_\eta > 1$ the flow becomes super-critical, i.e. the particle speed overtakes the wave's celerity and wave breaking commences. Several authors have explored use of various wave breaking criteria in practical situations. For example, the works (Bacigaluppi et al. 2020), and (Wu and Nepf 2002) present such studies. Recently, it was shown in Varing et al. (2021) that for $Fr|_\eta > 0.85$, waves are inevitably approaching the stage of breaking, i.e. a point of no return is passed and the wave will sooner or later break. However, it should be noted that the celerity refers to the shallow water celerity under hydrostatic conditions. In a single space dimension, the fluid particle velocity may be found in a straightforward manner in Boussinesq systems (Bjørkavåg and Kalisch 2011), and it can be used to pinpoint wave breaking quite accurately (Hatland and Kalisch 2019). In two spatial dimensions, the actual celerity under moderately dispersive waves is difficult to find and usually requires a Lagrangian post-processing method. Hence, the use of $C = \sqrt{gh}$ is not a perfect but still a very reasonable estimate.

2.4 Closure of wave breaking

It is possible to use the well-known concept of an eddy viscosity scheme for extension of Boussinesq-type equations. While some codes deactivate the dispersive terms in order to avoid the blowup of the solution, we follow a different approach. If active wave breaking is detected, an eddy viscosity (diffusive) term is added to the governing equations where it diffuses the wave breaking front so that the slope of the free surface cannot develop a sharp shock-front. This, in turn, prevents the dispersion terms from pumping excessive amounts of energy into the wave face and causing a blow-up. This closure approach goes back to the work of Zelt (1991) and Kennedy et al. (2000) who applied the following diffusive term to the momentum equations

$$\mathbf{R_b} = \begin{bmatrix} 0 \\ 2(\nu_t H u_x)_x + [\nu_t H(u_y^\alpha + v_x^\alpha)]_y \\ 2(\nu_t H v_y)_y + [\nu_t H(u_y^\alpha + v_x^\alpha)]_x \end{bmatrix}. \tag{6}$$

In one spatial dimension, the mixed-derivatives, xy-terms disappear, and the diffusive term in the x-momentum equation reduces to

$$\mathbf{R_b} = \left[\nu_t H u_x^\alpha \right]_x. \tag{7}$$

The diffusion terms in the momentum equations of (6) and (7) involve the time-varying quantity of eddy viscosity ν_t, which sets the magnitude or strength of the diffusion term. However, the magnitude of the dissipative term not only depends on the local variables (H, u, v) but also on the entire flow field which is evolving over time. It is therefore necessary to provide a physical basis for ν_t to better estimate its magnitude.

One way to determine the quantity ν_t is by using the turbulent kinetic energy (TKE) as a proxy. The following relation between TKE and ν_t was suggested by Prandtl (1945) and Kolmogorov (1942) as

$$\nu_t = C_\nu \sqrt{k}\, \ell_t \tag{8}$$

where $C_\nu = 0.55$ and ℓ_t is the mixing length and chosen as $\ell_t = h$.

In some previous works such as Nwogu (1996) or for example (Zhang et al. 2014) and (Kazolea and Ricchiuto 2018), a transport equation for turbulent kinetic energy given by Pope (2000) was used to determine its spatial and temporal variation, which is then used for (8) and subsequently in (6). Even though TKE is produced locally where the wave breaking criterion (e.g. the one presented in Sect. 2.3) is exceeded, the term (8) is applied over the entire computational domain. In contrast to previous studies such as Kennedy et al. (2000), the expression (8) can take on non-zero values even when the wave breaking criterion is locally not exceeded. It is possible that TKE remains in the system for some time or that it is advected outside the surf zone. The term can be seen as modelling the whitewater region which is intense and very turbulent at the location of wave breaking but not outside of the region of active breaking.

The governing equation, first used by Nwogu (1996), goes back to a single-equation turbulence closure model for TKE given as

$$k_t = -\mathscr{A} - \mathscr{E} + \mathscr{P} + \mathscr{D}, \tag{9}$$

where $\mathscr{A}$, $\mathscr{E}$, $\mathscr{P}$, $\mathscr{D}$ denote advection, elimination/destruction, production, and diffusion of TKE, denoted by k. The TKE term has units of energy $[m^2/s^2]$.

The model assumes the rate of production of turbulent kinetic energy to be proportional to the vertical gradient of the horizontal water particle velocity at the wave crest.

The turbulence is produced only in a cell where the horizontal velocity at the wave crest exceeds a particular criterion such as the one detailed in Sect. 2.3. Therefore, only $\mathscr{P}$ is calculated locally, whereas the other terms in Eq. (9) are computed throughout the entire domain.

The terms of Eq. (9) are below:

The TKE advection term is defined as

$$\mathscr{A} = \left[u k_x + v k_y \right]. \tag{10}$$

The derivatives k_x and $v k_y$ are approximated with a one-sided upwind approach. The TKE elimination/destruction terms is denoted as

$$\mathscr{E} = C_D \frac{k^{3/2}}{\ell_t}. \tag{11}$$

The TKE diffusion term is small and based on the kinematic viscosity of water, ν. Here, we use $C_D = C_\nu^3$, and $\nu = \frac{\mu}{\rho} \approx 0.001\,[m^2/s]$.

$$\mathscr{D} = \nu(k_{xx} + k_{yy}), \tag{12}$$

with ν_3 as the kinematic viscosity of water. The last term is the production of TKE. Since it is only computed in a cell where the criterion in Eq. (5) is exceeded. The parameter B works as a flag and takes on values of either 0 or 1. We use the formulation used by Nwogu (1996) with a modification consistent with the fundamental derivation of the production term of TKE as

$$\mathscr{P} = B \frac{l_t^2}{\sqrt{C_d}} \left[|u_z|_\eta^2 + |v_z|_\eta^2 \right]^{\frac{3}{2}}, \tag{13}$$

where the vertical gradients of the horizontal flow velocities u and v are taken at the free surface η. The vertical gradients of the horizontal velocities can be computed from the truncated Taylor series expansion in combination with the irrotationality condition $(w_x = u_z, w_y = v_z)$ as

$$\begin{aligned} u_z|_\eta &= -\eta \left[u_{xx} + v_{xy} \right] - \left[(hu)_{xx} + (hv)_{xy} \right] \\ v_z|_\eta &= -\eta \left[u_{xy} + v_{yy} \right] - \left[(hu)_{xy} + (hv)_{yy} \right] \end{aligned} \tag{14}$$

Once the wave breaking criterion is flagged, the vertical gradients of the horizontal velocities in Eq. (14) are the primary contributors to the magnitude of $\mathscr{P}$. Energetic breaking, such as encountered in plunging breakers, leads to an increase in the vertical gradient of the horizontal velocities under the wave crest and consequently to an increase in u_z and v_z.

3 Numerical experiments and statistical analysis

The *BOSZ* model was used to create 4 h data sets of wave and run-up conditions for altogether 36 scenarios, including 18 sea states and two different slopes. The sea states were constructed using time-series realizations of appropriate spectra and applying these as boundary conditions through boundary forcing of the equations. The 18 sea states include three different peak periods ($T_p = 12$ s, $T_p = 15$ s and $T_p = 18$ s), and six different values of significant waveheight H_s, ranging from 0.5 to 3.0 m. Finally, two different coastal slopes (1:20 and 1:2) were tested (see Fig. 2). Bottom friction is intentionally omitted to avoid unnecessary decay of the waves over the gentle slope. This ensures that the results are rather on the conservative side, since friction has a more significant effect on gentle slopes than on steep ones. The zero friction assumption is also realistic with respect to an application to a site such as the Norwegian coast where the exposed steep-sloping bedrock is naturally rather smooth and often even overgrown by algae which makes it very slippery.

Time series were recorded for both offshore location and for run-up height. For the offshore signal, a standard zero-crossing segmentation was applied, while for the run-up signal, each time series was reduced to a series of run-up heights by determining maximum elevation of the waterline. The offshore time series yielded a Rayleigh distribution in waveheight as expected. The run-up height for the gentle slope also followed a Rayleigh distribution although less accurately than the offshore values. The run-up height on the steep slope featured heavy tails as already intimated in the introduction.

As an example, we take a close look at the results for a relatively benign sea state with significant waveheight $H_s = 1$ m and peak period $T_p = 15$ s. Figure 3 shows the sea
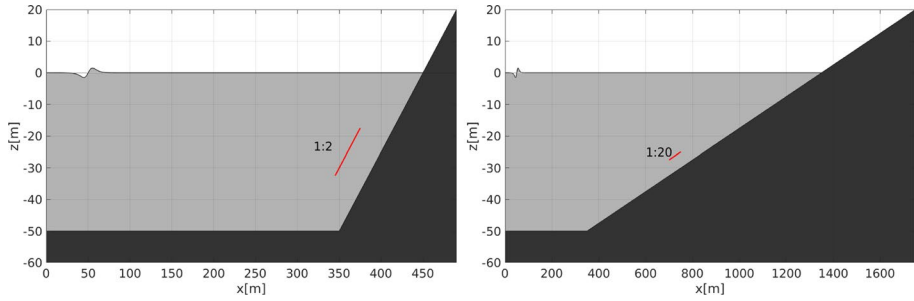
Fig. 2 Experiments were run on two slopes. The steep slope had a 1:2 aspect ratio, while the gentle slope had a 1:20 aspect ratio. The left boundary includes a sponge with an extent of 150 m, up to the location of the wavemaker at a distance of 150 m from the left boundary. In both cases, the slope starts at a distance of 350 m from the left boundary
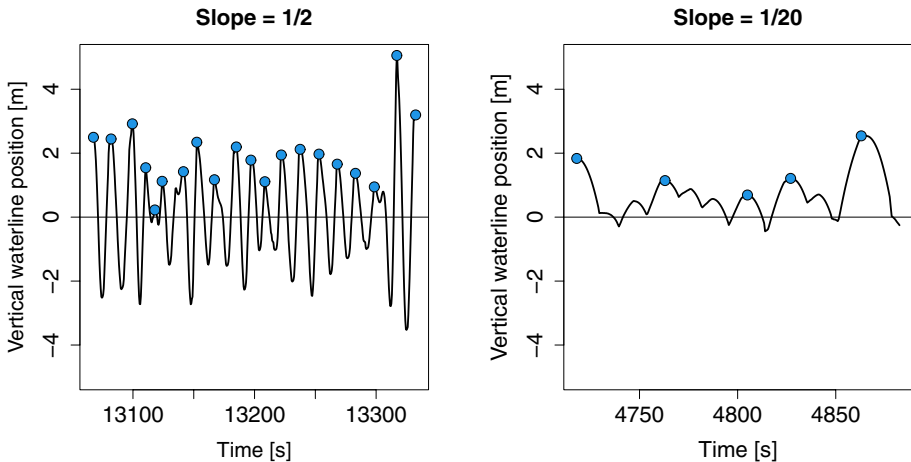

Fig. 3 This figure shows a 400-second data burst of the run-up time series for the steep 1:2 slope (left panel) and 200-second data burst of the run-up time series for the gentle 1:20 slope (right panel). In both panels, the sea-state parameters are $H_s = 1.0$ m and $T_p = 15$ s. The blue dots indicate the high watermark for each individual run-up. In the left panel, it can be seen that the maximum of each run-up is higher, and peaks are more frequent. On the other hand, on the gentle slope in the right panel, run-up peaks are less frequent and take more time to build up. The near 5 m run-up at ~ 13316 seconds appears exceptional and unexpected given the otherwise lower maximum run-ups of about 2 meters in the time series on the left

elevation at the point where the free surface meets the sloping beach (i.e. the waterline). The figure shows 300-second data bursts of the vertical position of the waterline for the two slopes considered. From this figure, it can be seen that run-up peaks appear in rapid succession on the steep beach (left panel). On the other hand, for the gentle beach shown in the right panel, run-up peaks are much less frequent and take more time to build-up. It can also be seen that large run-up can appear unexpectedly on the steep slope. Indeed, as can be seen in the left panel of Fig. 3, after a sequence of relatively low run-ups (less than 2.2 m) for about three minutes (between 13050 and 13350 s), a large run-up of almost 5 meters appears at about 13316 s. It is exactly this largely unexpected change in behavior which makes steep slopes so treacherous.

Figure 4 displays the full 4 h time series of the run-up elevation. The mean run-up across all run-up highs during this 4 h dataset is 1.52 meters for the 1:2 slope, only slightly higher than the mean of 1.02 for the gentle 1:20 slope. The third quartile is 2.08 meters for the steep 1:2 slope, also higher but only slightly so than then the 1.40-meter third quartile of the gentle 1:20 slope. Outliers however deserve special attention. Here and through the paper, an observation is referred to as an outlier if it is beyond 1.5 times the inter-quartile range of the distribution (Tukey's rule), such as explained in Gather and Becker (1997). Specifically, the steep slope has 10 outliers versus 0 outliers for the gentle slope Most of the outliers for the steep slope are in the 4 meter range, but one run-up reaches 5 meters. In contrast, the maximum for the gentle beach is 2.54 meters. The data are summarized for this and several other cases in Table 1.

Figure 5 displays the distribution of two further exemplary cases: the distribution of run-up heights under calm-sea conditions with distant swell arriving (significant wave height $H_s = 1$ m and period $T = 18$ s) and under $H_s = 2$ m, when the slope is gentle (1:20) or steep (1:2). When $H_s = 1$ m, on a 1:2 slope, the inter-quartile range is about 0.2 m larger than for the 1:20 slope (1.15 versus 0.90) and the difference between the 98 percentile and the median is about 0.5 m larger (1.88 versus 1.35). This also indicates that a steeper slope is associated with a greater probability of extreme events (right-tail elongation).

Such differences are even more pronounced when $H_s = 2$ m. On the 1:2 slope, the inter-quartile range is about 1 m larger than for the 1:20 slope (2.6 versus 1.5), and the difference between the 98% percentile and the median is about 2.2 m larger (3.70 versus 1.52). Indeed, even for agitated sea states, the steep slope can be dangerous because the highest highs of the run-up can be unexpectedly much higher than surrounding large events. In fact, considering again Fig. 5, the highest run-ups for the 2-meter sea state are over 8 meters, much higher than the 3rd quartile of 4.48 meters. In contrast, the same sea state on the gentle 1:20 slope has no outliers at all.

Figures 6 and 7 systematically compare the quantiles of the empirical run-up distributions, under different values of H_s and peak periods T, with the quantiles expected
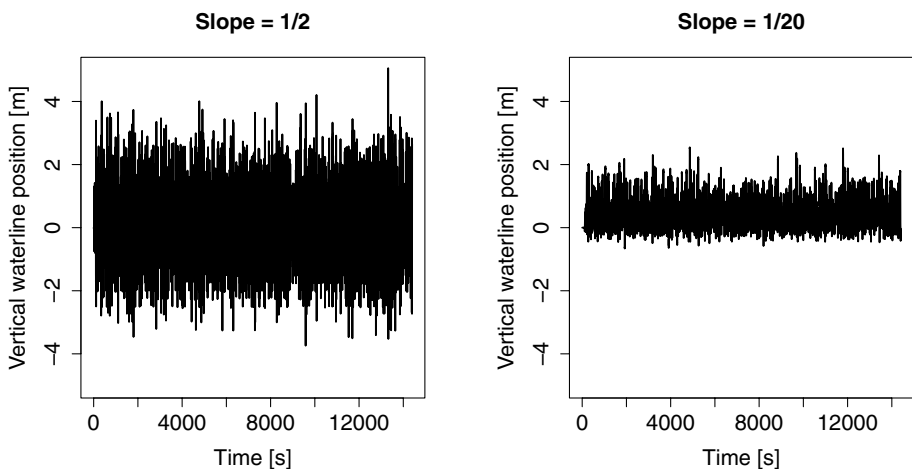

Fig. 4 Full 4 h time series of run-up heights for the steep 1:2 slope (left panel) and for the gentle 1:20 slope (right panel). The sea-state parameters are the same as in Fig. 3: $H_s = 1.0$ m and $T_p = 15$ s. In the left panel, it can be seen that maximum run-up is higher, and peaks are more frequent. On the other hand, on the gentle slope in the right panel, run-up peaks are less frequent, and much lower
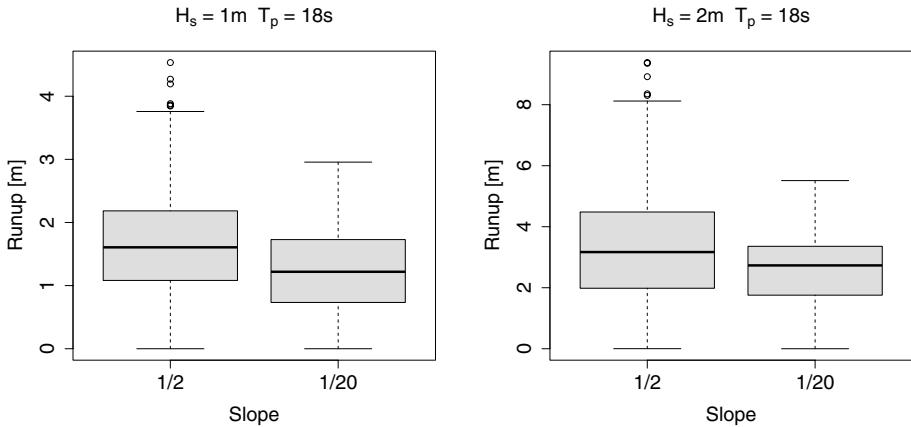
Fig. 5 Box-and-whisker diagrams of the distribution of run-up heights at a 1:20 coastal slope (left) and a 1:2 coastal slope (right) for two specific sea states: significant waveheight $H_s = 1$ m and peak period $T_p = 18$ s (left) and $H_s = 2$, $T_p = 18$ s (right). Boxes are drawn from the first to the third quartile of the distribution, with a bold horizontal line indicating the median. Dots indicate outliers, that is observations beyond 1.5 times the inter-quartile range

under a Rayleigh distribution with parameter $1/H_s$. In the case of a steep slope (1:2), higher-order quantiles are increasingly under-estimated by the quantiles expected under a Rayleigh assumption. In other words, the probability of the occurrence of extreme events is systematically under-estimated, with a bias that increases with H_s and (at a moderate extend) T. In contrast, under the case of a gentle slope (1:20), observed quantiles are well approximated by their Rayleigh counterparts, regardless of level reached by H_s.

4 Discussion

In the present work, we have focused on wave shoaling on a steep 1:2 slope where the steep bathymetry has a decisive effect on the evolution of the incoming ocean waves and on the resulting run-up. 36 scenarios were simulated, resulting in a 4-h time series of waterline movement for each case. The time series were analyzed statistically, and the main results are shown in Figs. 6 and 7. These figures show that on gentle slopes, the run-up distribution is close to a Rayleigh distribution (similar to the Rayleigh distribution of waveheights in a wave spectrum). On the other hand, the run-up distribution on steep slopes deviates significantly from the Rayleigh distribution with a bias that increases with the sea severity (increasing H_s). Similar results have been obtained under shorter computational times (1 and 2 h), but are not shown here.

As an example, we have analyzed the particular case of a sea state with significant waveheight $H_s = 1$ m and peak period $T_p = 15$ s. Considering Fig. 3, we see that on the steep slope, a single run-up of 5 meters occurs during a 4 h period. The 3rd quartile is 2.58 meters, and there are several outliers of about 4 meters run-up height. After observing the wave action for an hour, an observer may position herself in a location convenient for viewing, but above the ca. 4 meter highest run-up observed during a one-hour assessment period. The 5-meter run-up will then be completely unexpected, and may pose an
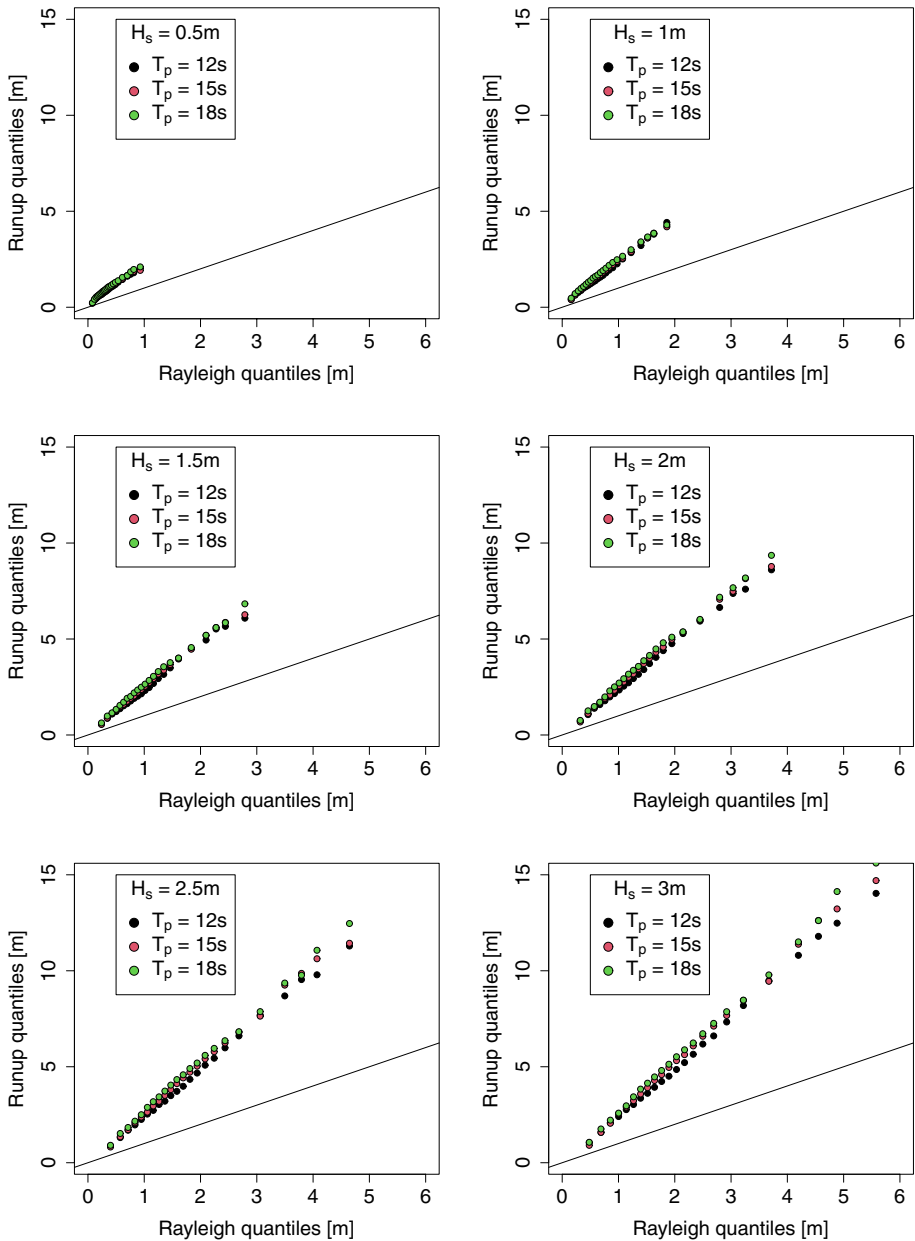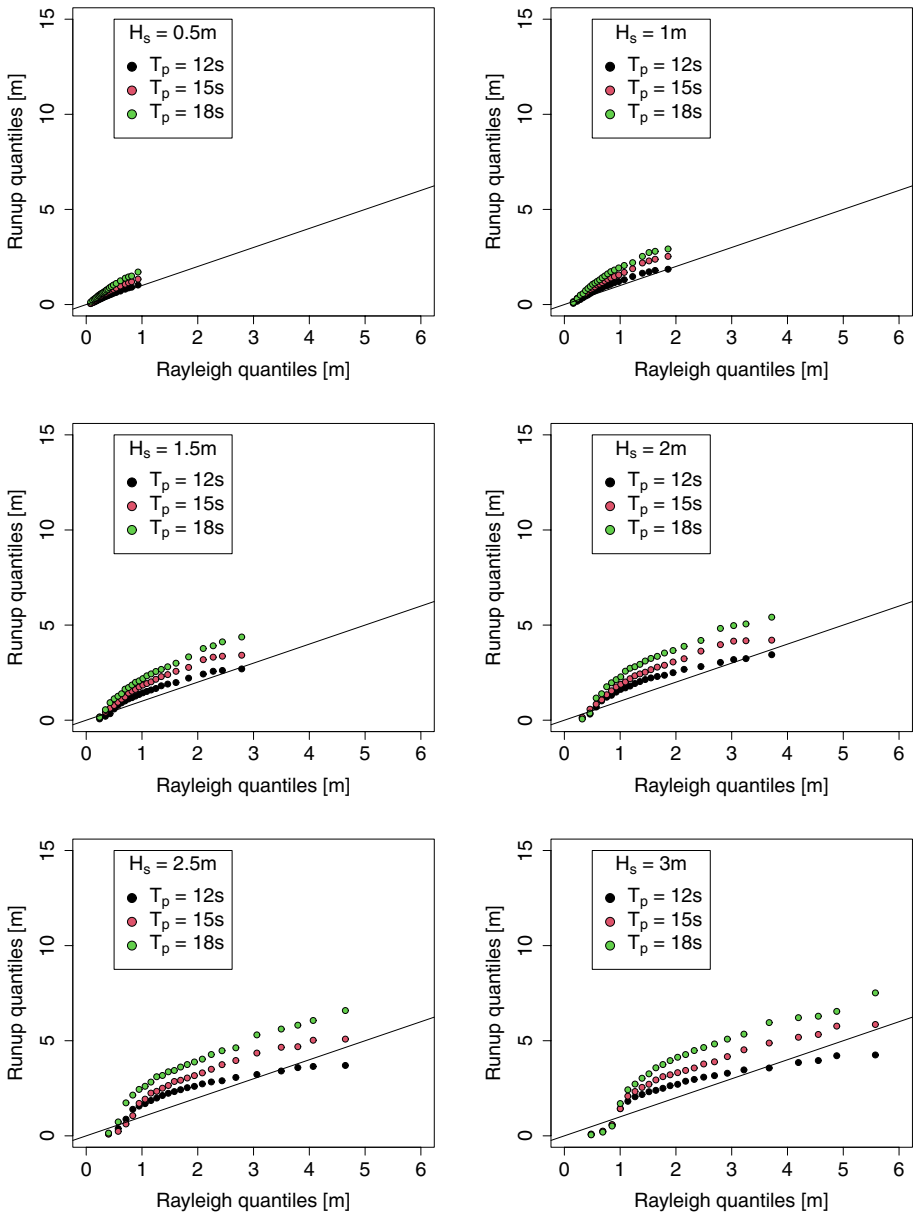
Fig. 6 Slope 1:2. Empirical quantiles of run-up heights versus Rayleigh quantiles (theoretical quantiles assuming a Rayleigh model) for 6 × 3 different sea states, obtained from 6 different values of significant waveheight H_s and 3 different values of peak period T_p. Quantiles are of order p from 5 to 99.9% in increments of 5% plus 98, 99, 99.5, 99.9%. Departures from the diagonal (indicated by a black line) indicate that higher empirical quantiles are increasingly larger than expected

Fig. 7 Slope 1:20. Empirical quantiles of run-up heights versus Rayleigh quantiles (theoretical quantiles in a Rayleigh model) for 6 × 3 different sea states, obtained from 6 different values of significant waveheight H_s and 3 different values of peak period T. Quantiles are of order p from 5 to 99.9% in increments of 5% plus 98, 99, 99.5, 99.9%. Departures from diagonal (the black line) are insignificant

imminent threat to the life and safety of the observer. As already discussed in the introduction, such incidents have happened, and are still happening for example in Norway Roxborough (2011).

Table 1 Run-up height during a four-hour simulation

Slope	T_p	H_s	Median	Mean	3rd Quartile	Maximum	# Outliers
1/2	12 s	0.5 m	0.81	0.78	1.06	2.12	7.00
		1.0 m	1.49	1.38	1.93	4.59	21.00
		1.5 m	2.22	2.02	2.94	6.70	16.00
		2.0 m	2.98	2.72	4.04	9.31	10.00
1/2	15 s	0.5 m	0.86	0.84	1.12	2.32	4.00
		1.0 m	1.58	1.52	2.08	5.06	10.00
		1.5 m	2.35	2.23	3.18	7.16	9.00
		2.0 m	3.15	3.01	4.31	9.89	7.00
1/2	18 s	0.5 m	0.90	0.88	1.15	2.19	7.00
		1.0 m	1.66	1.61	2.18	4.53	6.00
		1.5 m	2.45	2.34	3.31	6.83	3.00
		2.0 m	3.28	3.17	4.48	9.38	5.00
1/20	12 s	0.5 m	0.36	0.35	0.51	1.04	2.00
		1.0 m	0.76	0.78	1.06	1.90	0.00
		1.5 m	1.21	1.27	1.67	2.73	0.00
		2.0 m	1.69	1.80	2.30	3.51	0.00
1/20	15 s	0.5 m	0.50	0.49	0.70	1.40	2.00
		1.0 m	1.01	1.03	1.40	2.54	0.00
		1.5 m	1.56	1.62	2.15	3.43	0.00
		2.0 m	2.05	2.18	2.79	4.22	0.00
1/20	18 s	0.5 m	0.65	0.61	0.88	1.79	2.00
		1.0 m	1.22	1.22	1.73	2.96	0.00
		1.5 m	1.90	1.99	2.56	4.43	0.00
		2.0 m	2.49	2.73	3.36	5.51	0.00

This table shows the median, mean 3rd quartile, maximum and number of outliers for a number of sea states

In many previous studies of extreme wave events in shallow waters, the bathymetry is not the decisive factor in the development of the event. Large waves in the nearshore zone are the subject of Soomere and Engelbrecht (2006) as well as Soomere (2010), where the authors cite wave interactions as a possible mechanism for freak wave development. In Zhang et al. (2019), both laboratory experiments and numerical computations are leveraged to study the development of unusually large waves. A list of freak wave events in shallow waters, but not necessarily at beaches is given in Didenkulova et al. (2006) and also in Nikolkina and Didenkulova (2011). At gentle beaches, large run-up may occur due to a confluence of large swell and an infra-gravity wave signal. Such wave are sometimes called sneaker waves (García-Medina et al. 2018), and are also included in Nikolkina and Didenkulova (2011) and in Didenkulova etal. (2006). One previous work where strong influence of the bed topography on the wave conditions was found was the in-depth study of Stefanakis et al. (2011). The authors discovered resonant conditions due to irregular bathymetry, but the overall slope used was still much less steep than the 1:2 slope considered here.

Comparing run-up behavior at a steep slope to a gentle slope, one can conclude that steeper slope generally feature higher run-up than gentle slopes for the same sea state. This is clearly brought out in Fig. 5 for two special cases, and also in Fig. 8 using $R_{2\%}$ across

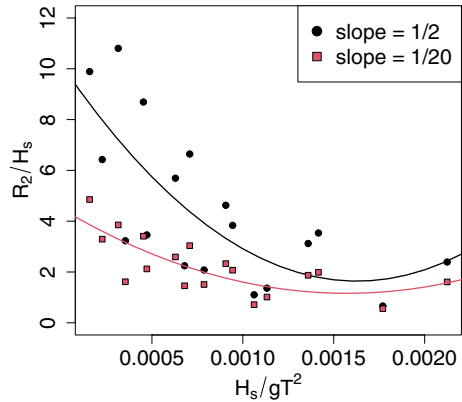| Coef.	Slope	
	$1/2$	$1/20$
C_1	1.02e+01	4.49e+00
C_2	-1.05e+04	-4.24e+03
C_3	3.22e+06	1.35e+06

Fig. 8 Plot and fit of 98 percentile $R_{2\%}$, normalized by significant wave height H_s vs. wave steepness H_s/T_p normalized by gT_p, where $g = 9.81$ m/s is the gravitational acceleration, using the formula (2). The black dots and the red squares are respectively the data under a 1/2 and a 1/20 slope, respectively, fitted by two least squares curve, with coefficients displayed in the left-hand side table. Both steep slope (1:2, left panel) and gentle slope (1:20, right panel) feature higher values of $R_{2\%}$ for smaller wave steepness (contrary to what one might expect). It is also clear that the steeper slope features higher overall run-up (by a factor of more than 2) than the gentle slope

all test cases. One interesting aspect of the data shown in Fig. 8 is that run-up is generally higher for sea states with lower overall wave steepness. One possible explanation for this feature is that steeper waves tend to break before they reach the shore so that the waves arriving at the beach are already tempered by wave breaking. Such behavior could be even more pronounced in the case of a reef or large shoals in front of the coast. For example, it was stated in Pelinovsky et al. (2013) that reefs can act as natural shore protection as the steepest waves are prone to break at the reef, and before reaching the shore. On the other hand, steep bathymetries such as reefs can also trigger large wave events in shallow water (Kharif et al. 2008). If large wave do reach the shore, large run-up is of course also possible, and for slopes steeper than 1:2, the run-up may be even more extreme (Kharif et al. 2008).

5 Conclusion

The numerical phase-resolving nearshore wave model BOSZ has been used to provide several hours of wave and run-up data on a gentle slope (1:20) and on a steep slope (1:2). Sea states ranging from 0.5 m significant waveheight to 3.0m significant waveheight were applied as an offshore condition. Statistical analysis was used to discern the distribution of run-up heights (i.e. the highest level of the waterline at the shore during one wave event) for a given sea state. The main findings are as follows. First, it is clear that on average, the steeper slope features higher run-up for all conditions investigated here. This can be observed visually such as for example in Figs. 3 and 4, but it can also be understood by comparing the 98 percentile $R_{2\%}$ as shown in Fig. 8. While the 98 percentile $R_{2\%}$ is commonly used in coastal engineering, it does not tell a complete story for the steep slope as it can be seen from Fig. 6 that higher quantiles diverge rapidly from the usual Rayleigh distribution, and outliers are much more common than in the standard theory. It follows that large run-ups can always be expected at a steep

coast. Since observers are not usually aware of the large preponderance of extreme events, they are prone to be caught by surprise. Dangerous and unforeseen run-up events may happen both during calm seas or during agitated seas since an extreme run-up height is large mainly when compared to the mean of the preceding events.

Since the current work is of a theoretical nature, a natural next step would be to investigate what happens under actual conditions at the coast. Indeed, further work may be directed towards the conduction of field measurements in particular of run-up conditions at a test site with a steep slope and ocean swell arriving on a regular basis. Such measurements could be taken in a similar fashion as the campaign reported in Dodet et al. (2018) where pressure gauges were deployed at a rock coast. However, the cited study was conducted at a coast with a rather gentle slope. At sites with 1:2 or steeper slopes such as the west coast of Norway, obtaining accurate measurements would be a major challenge due to the extreme slope and small tidal range making it difficult to deploy in-situ devices.

Appendix 1: Validation of the TKE model

The performance of the TKE formulation for the wave breaking closure has been examined with various benchmarking tests. Here, we show the results from the Suzuki experiment with irregular waves breaking over a gentle slope. The original bathymetry was given with 0.1 m grid spacing, which posed no problem to any of the wave breaking criteria used so far. Deactivation of the dispersion terms works almost equally well as applying an eddy viscosity term with constant ν_t. However, this is mostly due to the rather coarse grid, which acts as a filter itself and prevents the development of instabilities even without particular treatment. This implies that comparable results can be obtained without any wave breaking criteria or treatment by only relying on the stability of the numerical solution and the inherent grid diffusion.

The performance of the TKE model in Eq. (9) can be best seen by refining the grid that would automatically force the solution into eventual instabilities along the wave fronts. Inappropriate treatment of wave breaking would lead at least to variations in the results among different grid spacing and, eventually, even to instabilities.

With the use of Eq. (9), converging results can be obtained up to 0.01 m grid spacing, which is 10 times as fine as the original bathymetry provided by Suzuki. The results vary very little with most of the variations induced by small variations in wave input as a result of the changes in grid spacing. This supports the point that the TKE formulation works consistently and helps to reduce mesh dependence (Figs. 9, 10, 11 and 12).

It should be noted that the performance of the wave breaking closure approach outlined in (2.4) is not very sensitive to the threshold chosen for the onset of TKE production. As detailed in (2.3), a threshold of $Fr|_\eta > 0.85$ was chosen based on suggestions from previous work. However, sensitivity tests have shown that slightly larger or smaller values hardly influence the results in terms of spectral energy distribution and run-up statistics.

Appendix 2: Wavemaker and model setup

The wavemaker builds on the theoretical concept presented in Wei et al. (1999). The idea behind this approach is to decompose an amplitude spectrum into multiple individual monochromatic waves and then generate them periodically with a random phase. We start off with the definition of the empirical Pierson-Moskowitz spectrum, for which only H_s and T_p
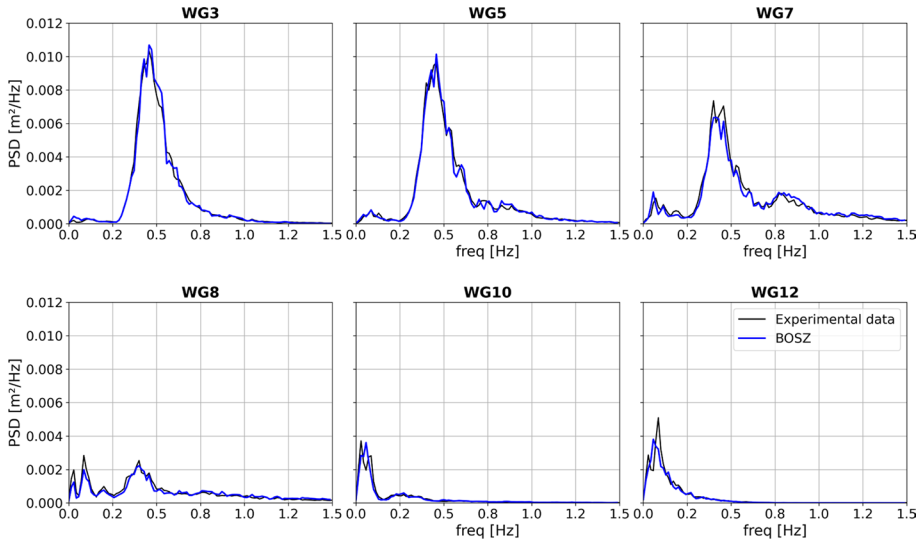
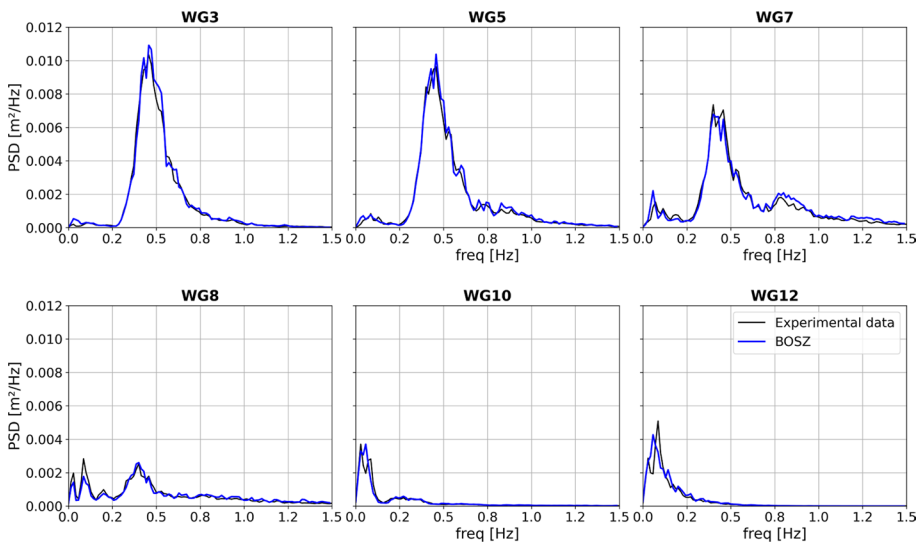**Fig. 9** Wave spectra from the Suzuki test with $\Delta x = 0.1\,m$

Fig. 10 Wave spectra from the Suzuki test with $\Delta x = 0.05\,m$

have to be known. The lowest frequency is 1/30 Hz which is commonly used as limiting frequency of the gravity wave spectrum. The highest frequency depends essentially on the dispersion properties of the numerical model and its governing equation.

Many Boussinesq-type equation such as the one from Nwogu (1993), are suitable for wave numbers up to around π. The solution does not break down for shorter waves but starts developing errors in the wave celerity. To ensure a proper representation of the spectrum and to avoid errors in the dispersion, we truncate the spectrum at $kh = \pi$, which
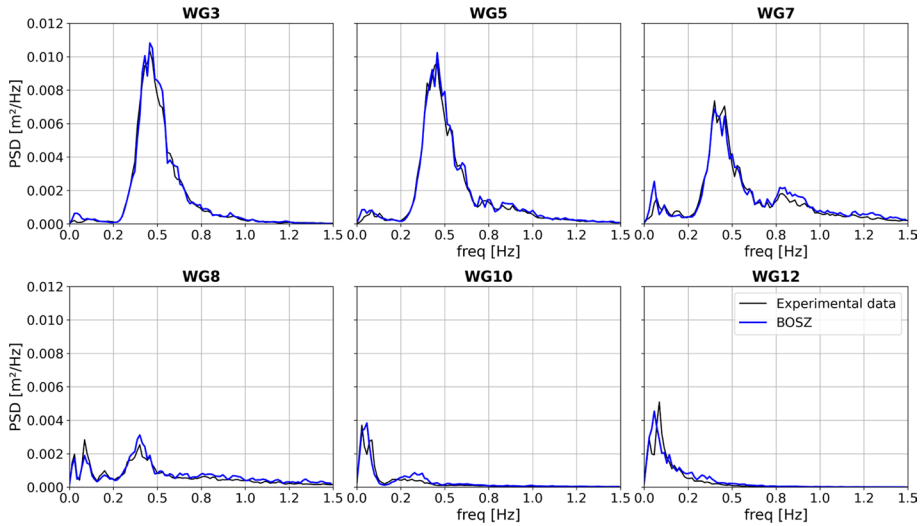
Fig. 11 Wave spectra from the Suzuki test with $\Delta x = 0.01\,m$
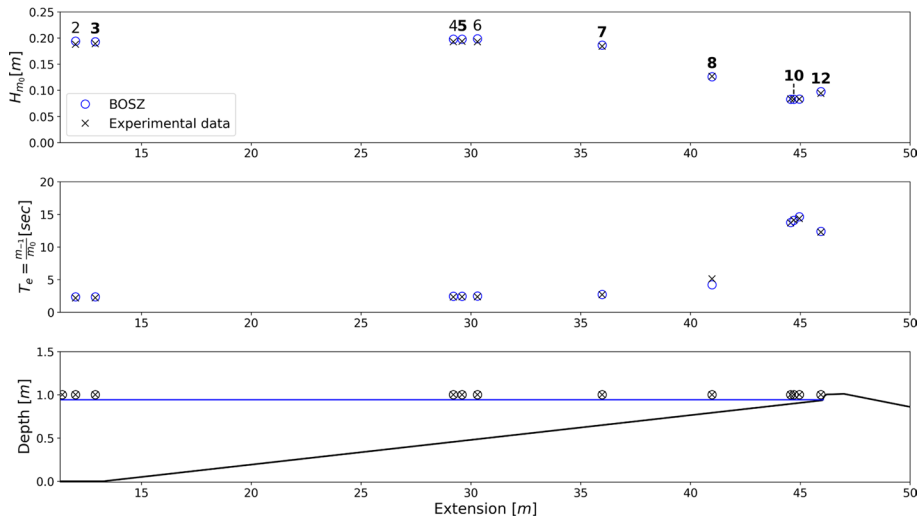
Fig. 12 Significant wave heights and energy periods from the Suzuki test with $\Delta x = 0.05\,m$ ($\Delta x = 0.1\,m$ and $\Delta x = 0.01\,m$ not shown)

corresponds to a frequency of 1/8 Hz. The spectrum is then divided into equally-spaced frequency bins between 1/30 and 1/8 Hz.

The width of the frequency bins depends essentially on the computed time in the model run. It is crucial that the time series resulting from the superposed monochromatic waves does not repeat (recycle) over the course of the computation. Otherwise artificial wave groups can contaminate the solution. With four hours of computed time, Δf is 0.0000694 Hz. Subdivision of the spectrum between to defined lower and upper frequency

limit results in 1317 frequency bins. Logically, a longer or shorter computed time would not affect the range of frequencies but the frequency bin width and consequently the total number of waves in the generation. The wave phases are initially set as random; however, the set of random phases is kept constant over all model runs to ensure repeatability of the computations. Once the waves are generated, they move away from the center of the source in both directions. The offshore propagating waves are immediately absorbed by a sponge layer that mimics an open ocean boundary condition and that would also absorb reflected waves from the slope, if there were any. The use of an empirical spectrum is convenient for this study as it allows for the simulation of a wide range of sea states in a controlled manner that would otherwise be difficult to obtain from buoy measurements.

The model runs were carried out over a regular Cartesian grid with $\Delta = \Delta y = 0.5$ m. The offshore water depth is of uniform 50 m depth until the toe of the slopes at 350 m from the left boundary. The left boundary also includes a sponge with an extent of 150 m (300 grid cells), up to the center location of the wavemaker. Due to the different slopes, the numerical domain are of different length and hence, the computations of the scenarios with the 1/20 slope take longer than the model runs for the 1/2 slope. The wet/dry boundary is handled by the TVD-Riemann solution where a minimum water depth of 10E-4 m is used as threshold. As suggested in other studies such as Pinault et al. (2020) a larger threshold than the one for the numerical differentiation between wet and dry cells should be applied to the run-up limit. Here, the run-up limit is identified where the flow depth drops below 0.05 m.

Declarations

Conflict of interest The authors have no relevant financial or non-financial interests to disclose.

Ethical approval Not applicable.

References

Ahrens JP (1981) Irregular wave runup on smooth slopes. Tech. rep, Coastal Engineering Research Center Fort Belvoir VA

Bacigaluppi P, Ricchiuto M, Bonneton P (2020) Implementation and evaluation of breaking detection criteria for a hybrid Boussinesq model. Water Waves 2(2):207–241. https://doi.org/10.1007/s42286-019-00023-8

Barthelemy X, Banner M, Peirson W et al (2018) On a unified breaking onset threshold for gravity waves in deep and intermediate depth water. J Fluid Mech 841:463–488. https://doi.org/10.1017/jfm.2018.93

Bjørkavåg M, Kalisch H (2011) Wave breaking in Boussinesq models for undular bores. Phys Lett A 375(14):1570–1578. https://doi.org/10.1016/j.physleta.2011.02.060

Bjørnestad M, Kalisch H (2020) Extreme wave runup on a steep coastal profile. AIP Adv 10(10):105205. https://doi.org/10.1063/5.0020128

David CG, Roeber V, Goseberg N et al (2017) Generation and propagation of ship-borne waves—Solutions from a Boussinesq-type model. Coast Eng 127:170–187. https://doi.org/10.1016/j.coastaleng.2017.07.001

Didenkulova E (2020) Catalogue of rogue waves occurred in the world ocean from 2011 to 2018 reported by mass media sources. Ocean Coast Manage 188(105):076. https://doi.org/10.1016/j.ocecoaman.2019.105076

Didenkulova E, Didenkulova I, Medvedev I (2023) Freak wave events in 2005–2021: statistics and analysis of favourable wave and wind conditions. Nat Hazards Earth Syst Sci 23(4):1653–1663. https://doi.org/10.5194/nhess-23-1653-2023

Didenkulova II, Slunyaev AV, Pelinovsky EN et al (2006) Freak waves in 2005. Nat Hazards Earth Syst Sci 6:1007–1015. https://doi.org/10.5194/nhess-6-1007-2006

Dodet G, Leckler F, Sous D et al (2018) Wave runup over steep rocky cliffs. J Geophys Res Oceans 123:7185–7205. https://doi.org/10.1029/2018JC013967

García-Medina G, Özkan-Haller HT, Ruggiero P et al (2018) Analysis and catalogue of sneaker waves in the US pacific northwest between 2005 and 2017. Nat Hazards 94:583–603. https://doi.org/10.1007/s11069-018-3403-z

Gather U, Becker C (1997) Outlier identification and robust methods. Robust Inference. Elsevier, Amsterdam, pp 123–143

Hatland SD, Kalisch H (2019) Wave breaking in undular bores generated by a moving weir. Phys Fluids 31(3):033601. https://doi.org/10.1063/1.5085861

Holman R (1986) Extreme value statistics for wave run-up on a natural beach. Coast Eng 9(6):527–544. https://doi.org/10.1016/0378-3839(86)90002-5

Kazolea M, Ricchiuto M (2018) On wave breaking for Boussinesq-type models. Ocean Model 123:16–39. https://doi.org/10.1016/j.ocemod.2018.01.003

Kennedy AB, Chen Q, Kirby JT et al (2000) Boussinesq modelling of wave transformation, breaking, and runup. J Waterway, Port, Coastal Ocean Eng 126:39–47

Kennedy DM, Stephenson WJ, Naylor LA (2014) Introduction to the rock coasts of the world. Geol Soc London, Memoirs 40(1):1–5

Kharif C, Pelinovsky E, Slunyaev A (2008) Rogue waves in the ocean. Springer Science & Business Media, Heidelberg

Kolmogorov A (1942) The equations of turbulent motion in an incompressible flow. Izvestia Acad Sci, USSR pp 56–58

Li N, Roeber V, Yamazaki Y et al (2014) Integration of coastal inundation modeling from storm tides to individual waves. Ocean Model 83:26–42. https://doi.org/10.1016/j.ocemod.2014.08.005

Lynett PJ, Gately K, Wilson R et al (2017) Inter-model analysis of tsunami-induced coastal currents. Ocean Model 114:14–32. https://doi.org/10.1016/j.ocemod.2017.04.003

Nikolkina I, Didenkulova I (2011) Rogue waves in 2006–2011. Nat Hazards Earth Syst Sci 11:2913–2924. https://doi.org/10.5194/nhess-11-2913-2011

Nwogu O (1993) Alternative form of Boussinesq equations for nearshore wave propagation. J Waterway, Port, Coastal Ocean Eng 119:618–638. https://doi.org/10.1061/(ASCE)0733-950X(1993)119:6(618)

Nwogu O (1996) Numerical prediction of breaking waves and currents with Boussinesq model. Coastal Eng Proc 1(25):4807–4820. https://doi.org/10.1061/9780784402429.374

Pelinovsky E, Didenkulova I, Mendez F et al (2013) Preface to sea hazards. Nat Hazards Earth Syst Sci 13:1063–1067. https://doi.org/10.5194/nhess-13-1063-2013

Pinault J, Morichon D, Roeber V (2020) Estimation of irregular wave runup on intermediate and reflective beaches using a phase-resolving numerical model. J Marine Sci Eng 8(12):993. https://doi.org/10.3390/jmse8120993

Pinault J, Morichon D, Delpey M et al (2022) Field observations and numerical modeling of swash motions at an engineered embayed beach under moderate to energetic conditions. Estuarine, Coastal and Shelf Sci 279:108143. https://doi.org/10.1016/j.ecss.2022.108143

Pope SB (2000) Turbulent flows. Cambridge University Press, Cambridge

Prandtl L (1945) Ueber ein neues formelsystem fur die ausgebildete turbulenz. nach. ges. wiss. gottingen, math. Phys Kl pp 6–18

Roeber V, Bricker JD (2015) Destructive tsunami-like wave generated by surf beat over a coral reef during typhoon Haiyan. Nat Commun 6(1):7854. https://doi.org/10.1038/ncomms8854

Roeber V, Cheung KF (2012) Boussinesq-type model for energetic breaking waves in fringing reef environments. Coast Eng 70:1–20. https://doi.org/10.1016/j.coastaleng.2012.06.001

Roeber V, Cheung KF (2012a) BOSZ (Boussinesq Ocean and Surf Zone model). NOAA Special Report, Proceedings and Results of the 2011 NTHMP Model Benchmarking Workshop pp 1–437

Roeber V, Cheung KF, Kobayashi MH (2010) Shock-capturing Boussinesq-type model for nearshore wave processes. Coast Eng 57(4):407–423. https://doi.org/10.1016/j.coastaleng.2009.11.007

Roxborough S (2011) Wave washes away two crew members on Norwegian film shoot. https://www.hollywoodreporter.com/movies/movie-news/veil-of-twilight-crew-members-washed-away-267079/

Shi F, Kirby JT, Harris JC et al (2012) A high-order adaptive time-stepping TVD solver for Boussinesq modeling of breaking waves and coastal inundation. Ocean Model 43–44:36–51. https://doi.org/10.1016/j.ocemod.2011.12.004

Soomere T (2010) Rogue waves in shallow water. Eur Phys J-Spec Top 185:81–96. https://doi.org/10.1140/epjst/e2010-01240-1

Soomere T, Engelbrecht J (2006) Weakly two-dimensional interaction of solitons in shallow water. Eur J Mech B Fluids 25:636–648. https://doi.org/10.1016/j.euromechflu.2006.02.008

Stefanakis TS, Dias F, Dutykh D (2011) Local run-up amplification by resonant wave interactions. Phys Rev Lett 107(124):502. https://doi.org/10.1103/PhysRevLett.107.124502

Stockdon HF, Holman RA, Howd PA et al (2006) Empirical parameterization of setup, swash, and runup. Coast Eng 53(7):573–588. https://doi.org/10.1016/j.coastaleng.2005.12.005

Varing A, Filipot JF, Delpey M et al (2020) Spatial distribution of wave energy over complex coastal bathymetries: development of methodologies for comparing modeled wave fields with satellite observations. Coastal Eng 169:103793. https://doi.org/10.1016/j.coastaleng.2020.103793

Varing A, Filipot JF, Grilli S et al (2021) A new definition of the kinematic breaking onset criterion validated with solitary and quasi-regular waves in shallow water. Coast Eng 164(103):755. https://doi.org/10.1016/j.coastaleng.2020.103755

Wei G, Kirby JT, Sinha A (1999) Generation of waves in Boussinesq models using a source function method. Coast Eng 36(4):271–299. https://doi.org/10.1016/S0378-3839(99)00009-5

Wong WY, Bjørnestad M, Lin C et al (2019) Internal flow properties in a capillary bore. Phys Fluids 31(11):113602. https://doi.org/10.1063/1.5124038

Wu CH, Nepf H (2002) Breaking criteria and energy losses for three-dimensional wave breaking. J Geophys Res Oceans 107(C10):41–1. https://doi.org/10.1029/2001JC001077

Zelt JA (1991) The run-up of nonbreaking and breaking solitary waves. Coast Eng 15:205–246. https://doi.org/10.1016/0378-3839(91)90003-Y

Zhang J, Benoit M, Kimmoun O et al (2019) Statistics of extreme waves in coastal waters: large scale experiments and advanced numerical simulations. Fluids 4:99. https://doi.org/10.3390/fluids4020099

Zhang Y, Kennedy AB, Donahue AS et al (2014) Rotational surf zone modeling for $O(\mu^4)$ Boussinesq-Green-Naghdi systems. Ocean Model 79:43–53. https://doi.org/10.1016/j.ocemod.2014.04.001